

# Arteriosclerosis Assessment Based on Single-Point Fingertip Pulse Monitoring Using a Wearable Iontronic Sensor

Yi Huang, Lingyu Zhao,\* Minkun Cai, Jiaqi Zhu, Liu Wang, Xinxing Chen, Yumin Zeng, Liqing Zhang, Jidong Shi,\* and Chuan Fei Guo\*

Arteriosclerosis, which appears as a hardened and narrowed artery with plaque buildup, is the primary cause of various cardiovascular diseases such as stroke. Arteriosclerosis is often evaluated by clinically measuring the pulse wave velocity (PWV) using a two-point approach that requires bulky medical equipment and a skilled operator. Although wearable photoplethysmographic sensors for PWV monitoring are developed in recent years, likewise, this technique is often based on two-point measurement, and the signal can easily be interfered with by natural light. Herein, a single-point strategy is reported based on stable fingertip pulse monitoring using a flexible iontronic pressure sensor for heart-fingertip PWV (hfPWV) measurement. The iontronic sensor exhibits a high pressure-resolution on the order of 0.1 Pa over a wide linearity range, allowing the capture of characteristic peaks of fingertip pulse waves. The forward and reflected waves of the pulse are extracted and the time difference between the two waves is computed for hfPWV measurement using Hiroshi's method. Furthermore, a hfPWV-based model is established for arteriosclerosis evaluation with an accuracy comparable to that of existing clinical criteria, and the validity of the model is verified clinically. The work provides a reliable technique that can be used in wearable arteriosclerosis assessment systems.

## 1. Introduction

Arteriosclerosis is a disease that often appears as the hardening and narrowing of artery walls.<sup>[1,2]</sup> Arteriosclerosis-induced cardiovascular diseases such as heart attack and stroke have been a primary cause of mortality worldwide.<sup>[3,4]</sup> Quantitative evaluations of arteriosclerosis have long been studied, among which the pulse wave velocity (PWV), a parameter in direct proportion to the vascular elastic modulus (or stiffening level),<sup>[5-7]</sup> is widely acknowledged as an effective indicator of arteriosclerosis risks.<sup>[8]</sup> PWV is usually determined by measuring the pulse transmit time (PTT) between two locations at a distance  $S$  of the same artery (two-point method), i.e.,  $PWV = S/PTT$ . Clinical PWV includes the brachial-ankle pulse wave velocity (baPWV)<sup>[9,10]</sup> and the carotid-femoral pulse wave velocity (cfPWV),<sup>[11,12]</sup> both measured with the two-point method. Such a measurement usually requires a skilled doctor operating a costly and bulky medical apparatus (e.g., Omron colin-automatic arteriosclerosis detector, which costs  $\approx 60$  k US

Y. Huang  
Department of Cardiology  
Southern University of Science and Technology Hospital  
(SUSTech-Hospital)  
Shenzhen 518071, China

L. Zhao, M. Cai, J. Zhu, C. F. Guo  
Department of Materials Science and Engineering  
Southern University of Science and Technology  
Shenzhen 518055, China  
E-mail: zhaoly@sustech.edu.cn; guocf@sustech.edu.cn


L. Wang  
CAS Key Laboratory of Mechanical Behavior and Design of Materials  
Department of Modern Mechanics  
University of Science and Technology of China  
Hefei 230026, China

X. Chen  
Shenzhen Key Laboratory of Biomimetic Robotics and Intelligent Systems  
Guangdong Provincial Key Laboratory of Human-Augmentation and  
Rehabilitation Robotics in Universities  
Southern University of Science and Technology  
Shenzhen 518055, China

Y. Zeng  
Department of Sports Center  
Southern University of Science and Technology  
Shenzhen 518055, China

L. Zhang  
Department of Endocrinology  
Southern University of Science and Technology Hospital  
(SUSTech-hospital)  
Shenzhen 518071, China

J. Shi  
Shenzhen Key Laboratory of Ultraintense Laser and Advanced Material  
Technology  
Center for Advanced Material Diagnostic Technology  
College of Engineering Physics  
Shenzhen Technology University  
Shenzhen 518118, China  
E-mail: shijidong@sztu.edu.cn

 The ORCID identification number(s) for the author(s) of this article can be found under <https://doi.org/10.1002/adhm.202301838>

DOI: 10.1002/adhm.202301838

dollars), partly because of the high demand for synchronization of the two sensors.<sup>[13,14]</sup> In addition, PWV measurement in hospitals often lasts for a short period of time, which may not be sufficient for accurate arteriosclerosis diagnosis.<sup>[15,16]</sup> Therefore, it is necessary to develop wearable devices that can provide continuous, non-invasive, and precise monitoring of PWV for arteriosclerosis assessment, and the technology is especially valuable in rural areas where apparatus and skilled doctors are lacking.

Flexible pressure sensors can convert mechanical stimuli into electrical signals and have been widely used to detect arterial pulse waves in a continuous mode because flexible devices can be conformally laminated on human skins for long-term monitoring.<sup>[17,18]</sup> Although great efforts on the measurement of PWV have been made,<sup>[19]</sup> existing PWV acquisition based on flexible pressure sensors still uses a two-point method, for which two sensors detect pulse waves at different arterial locations (mostly joints) simultaneously.<sup>[20]</sup> This technology, however, suffers from two drawbacks. First, body motions can severely affect the detection of pulse waves using wearable sensors laminated at joints. For example, radial artery pulse detection is the most widely used, but the signal often becomes undetectable when the wrist bends forward.<sup>[21]</sup> Second, the synchronization of signals from the two electrical recording channels causes further challenges in the design of circuit and algorithm.

An alternative solution is to develop a single-point PWV monitoring system using one flexible pressure sensor. However, constructing such a single flexible sensor-based wearable system is challenging—it requires high stability and reliability of the pulse wave detection, together with a valid computation of PWV based on the signal of one sensor. Here, we report single-point heart-to-fingertip PWV (hfPWV) measurement on the basis of a flexible iontronic pressure sensor for fingertip pulse detection. The sensor exhibits high-pressure resolution (the smallest pressure that the sensor can detect) on the order of 0.1 Pa and linear response that allow for the detection of characteristic peaks of the fingertip pulse, which was selected for further analysis due to its high stability upon hand gestures. We use Hiroshi's method for hfPWV measurement,<sup>[22]</sup> and develop a model that can be used to assess the level of arteriosclerosis based on the hfPWV values. Our study suggests that this single-point hfPWV measurement based on our flexible iontronic sensor is comparable to the traditional two-point method (based on baPWV) in terms of accuracy while being much simpler in the system buildup and operation. We expect our single-point method to be applied in portable and long-term daily monitoring systems of arteriosclerosis assessment.

## 2. Results and Discussion

### 2.1. Principle of the hfPWV Measurement

The pulse wave is the superposition of the forward pulse wave and the reflected pulse wave (Figure 1a). The forward pulse wave is formed as the heart ejects blood to the periphery,<sup>[23,24]</sup> while the interaction between the forward pulse and the micro-arteries leads to a centripetal reflection of blood, generating the reflected pulse wave.<sup>[20,25,26]</sup> The reflected pulse wave is constrained by the closed arterial valve, generating a secondary forward pulse wave (Figure 1a).<sup>[27,28]</sup> Therefore, the re-reflected pulse lags behind the initial forward pulse by twice the heart-fingertip length ( $S$ ) and

the time difference between them represents the round-trip time of the pulsed wave from heart to fingertip, defined as the heart-to-fingertip PTT (hfPTT). When arteriosclerosis occurs, PWV increases and hfPTT reduces (Figure 1a).

In Hiroshi's method, the acceleration pulse wave (APW), which is acquired through the quadratic differentiation of the original waveform by time, has been widely used since it reflects the axial driving force and the resistance to the arterial blood flow.<sup>[29,30]</sup> In this work, the pulse is detected using our iontronic sensor laminated at the fingertip. The APW shows a waveform of damped oscillation resulting from the repeated reflection of the heart valves (peaks in APW) and the capillaries at the fingertip (valleys in APW) (Figure 1b). Therefore, the round-trip time of the pulsed blood flow between heart and fingertip, or hfPTT, is identified as the time interval between the first two peaks, and the corresponding PWV value (hfPWV) can be calculated by dividing  $S$  with hfPTT.

The clinical assessment of arteriosclerosis, however, usually uses a different principle. The clinical methods apply a two-point method to detect PWV, by detecting pulses simultaneously at the brachial and ankle arteries. The PWV value, called baPWV, is computed as:

$$baPWV = \frac{L_b - L_a}{\Delta T} \quad (1)$$

where  $L_a$  is the distance from the ankle artery to the aortic valve,  $L_b$  is the distance from the brachial artery to the aortic valve, and  $\Delta T$  is the time difference (Figure 1c).<sup>[31]</sup> Although this method is straightforward, it suffers from the high requirement in synchronization and unstable signal caused by joint motion.

### 2.2. Fabrication and Sensing Properties of the Iontronic Sensor and Its Performance in Fingertip Pulse Monitoring

In this study, we utilize iontronic pressure sensors that consist of a layer of microstructured ionic gel sandwiched between two flexible electrodes to detect fingertip pulse waves. These iontronic sensors create a tunable iontronic nanointerface through the contact between the microstructured ionic layer and the electrodes. An electric double layer forms at the interface, for which ions and electrons are at a nanoscale distance. As a result, an ultrahigh areal capacitance and a sensitive electromechanical response can be achieved. Upon loading, the contact area between the electrode and ionic layer increases to generate an increase in capacitive signal.<sup>[32,33]</sup> The microstructure of the ionic layer plays a key role in tuning the properties of the sensor. Signal saturation, a phenomenon that the increase of response gets slower, which is caused by the stiffening of soft materials, has long puzzled the field. Recently, a microstructure that utilizes an "intrafilling" effect (using holes and grooves to accommodate bulked protrusions and to relieve structure stiffening) has proven to be effective in relaxing the stiffening effect and further broadening the working range of flexible pressure sensors.<sup>[33]</sup> However, nonlinear response in such devices still exists.

The microstructure in this work can result in wide-range linear response of the iontronic sensor. This microstructure is a tilted, peanut-like pillar array with each pillar neighboring a

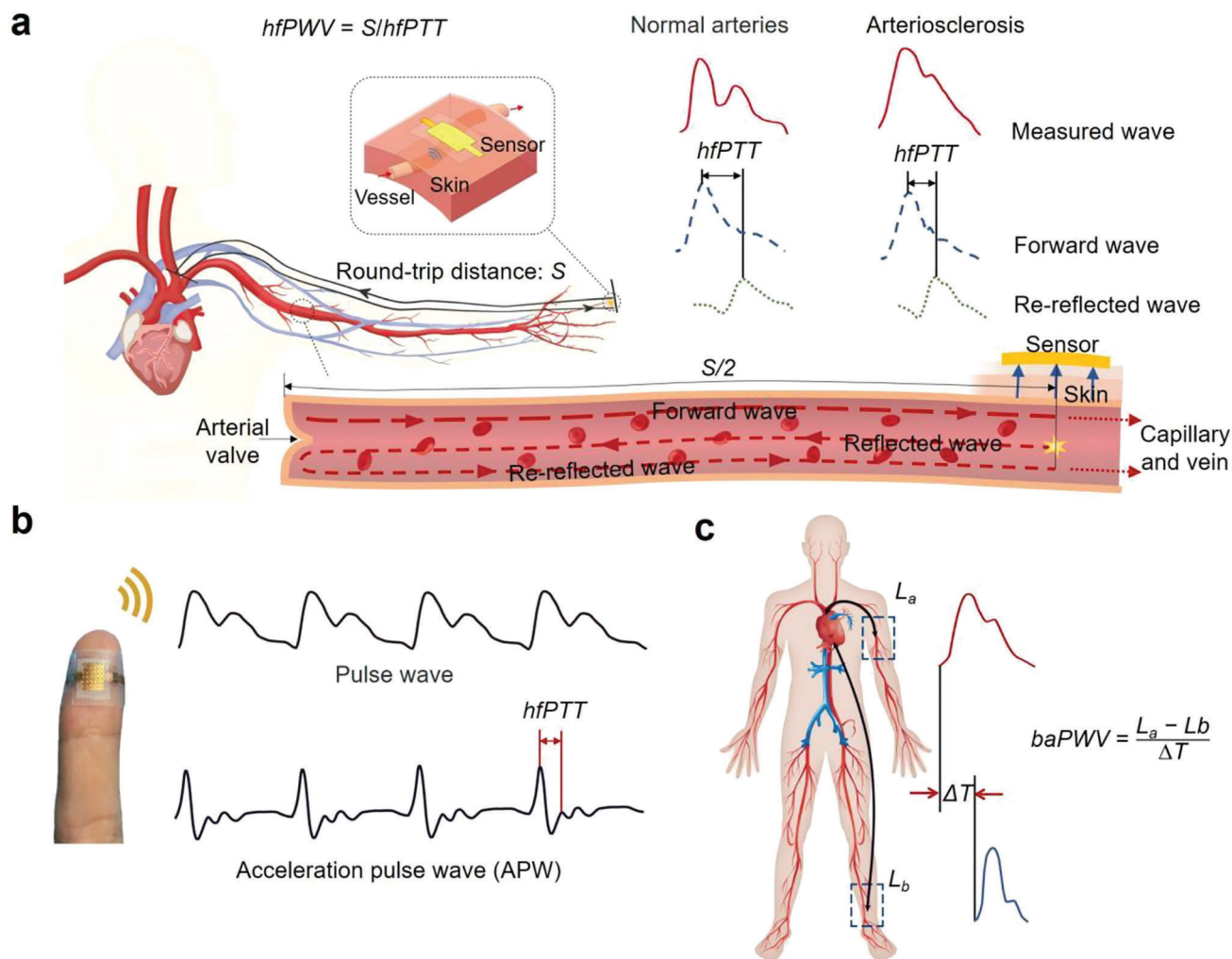


**Figure 1.** Single-point method for pulse wave velocity (PWV) measurement. a) Schematic illustration for the principle of hfPWV measurement. A flexible pressure sensor attached on a fingertip is used to detect pulse wave, from which hfPTT is extracted. b) Fingertip pulse wave and corresponding acceleration pulse wave. c) Principle of the baPWV measurement using a two-point method.

complementary-shaped groove (we call a peanut-groove structure). Such a design features linear response of sensitivity over a wide working range (0–150 kPa). The deformation of the peanut-groove structures under compressive loading is elucidated by finite element analysis (FEA), where a linear relationship between normalized iontronic contact area ( $A/A_0$ , where  $A$  is the actual contact area, and  $A_0$  is the original contact area before loading) and the applied pressure is observed (Figure 2a,b). Note that  $A/A_0$  has been widely acknowledged as a measure of the sensitivity ( $\Delta C/C_0$ ) of the iontronic sensor in the light of the supercapacitive nature of EDLs (i.e.,  $C-A$ ). The linearly increasing contact area is attributed to the buckling of the peanuts and the subsequent filling of the groove, i.e., the structure shows a high compressibility without exerting too much resistive force to the applied pressure. By contrast, a control structure with a tilted pillar in the absence of grooves (termed peanut-flat structure) has a lower compressibility and thus exhibits a rapidly increasing resistive force, leading to a nonlinear response between the contact area and applied pressure. Furthermore, a hemispheric structure that

cannot buckle shows even poorer compressibility and the lowest change of area.

The linear response caused by the peanut-groove structure is also verified in the experiment. The peanut-groove microstructure was fabricated by 3D printing (Figure 2c and Figure S1–2, Supporting Information), and encapsulated between two Au (100 nm)-polyimide electrodes to form a sensor. The sensor demonstrates high flexibility, which enables its attachment to curved skin (Figure S3, Supporting Information). In accordance with the simulation result, the output of the iontronic sensor shows high linearity with a correlation coefficient of  $R^2 \approx 0.999$  over a broad range of 0–150 kPa (Figure 2d). The high linearity is further verified in two demonstrations—in either stepwise-increased loadings, or random loadings (Figure S4a–d, Supporting Information).

Our sensor exhibits high pressure resolution under different preloads. Pressure-resolution determines the capability of a sensor to detect tiny pulse signals. Although pressure-resolution decays with applied preloads, it does not exceed 1 Pa within a

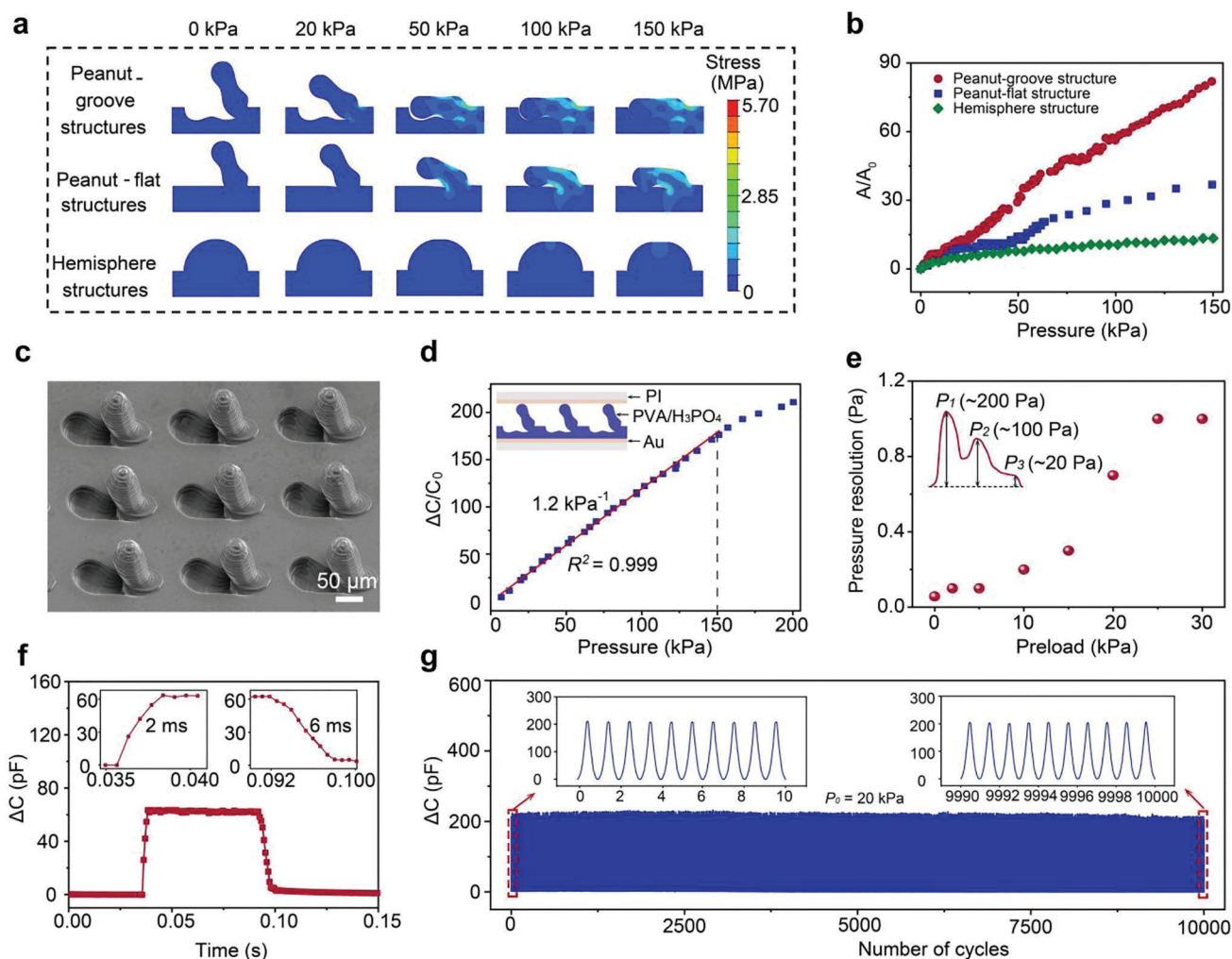


**Figure 2.** Principle, fabrication, and sensing properties of the iontronic pressure sensor. a) Finite element analysis (FEA) result showing the stress distribution of the peanut-groove structure, the peanut-flat structure, and hemispheric structures under pressures up to 150 kPa. b) FEA result of the change in contact area between the microstructured ionic layers and the electrode under pressures from 0 to 150 kPa. c) Tilt-view SEM image of the peanut-groove structured ionic gel. d) Normalized change in capacitance as a function of pressure (0 to 200 kPa). The inset shows the structure of the sensor. e) Pressure resolutions of the sensor at different basic pressures in the range of 0–30 kPa. f) Response time (2 ms) and relaxation time (6 ms) determined by applying and withdrawing a pressure of 6 kPa. Insets: magnification of the loading and releasing moments. g) Response of the sensor over 10000 cycles under a preload of 20 kPa.

preload range of 0–30 kPa. Specifically, the pressure-resolution reaches 0.2 Pa when the preload is less than 10 kPa (Figure 2e), which is the optimal preload for fingertip pulse monitoring that will be discussed hereinafter. The high pressure-resolution ensures that the sensor can well capture the characteristic peaks of the weak fingertip pulse. In addition to the high linearity and high pressure-resolution, the sensor exhibits a short response and relaxation time of 2 and 6 ms, respectively (Figure 2f). The rapid response-relaxation speed is sufficient for the sensor to resolve the short intervals between the characteristic percussion (P-), tidal (T-) and diastolic (D-) waves. The pressure sensor also demonstrates high stability over cycling. No significant change in signal magnitude is observed when the device is subjected to 10 000 loading-release cycles with a peak pressure of 20 kPa (Figure 2g). Our structure observation further confirms the stability of the sensor—the scanning electron microscopy inspec-

tion shows that the microstructures are not changed before and after the cyclic test (Figure S5, Supporting Information). The high stability in both electrical signal and microstructures indicates that the sensor can serve as a reliable pressure sensing device for the pulse monitoring applications.

### 2.3. Fingertip Pulse Monitoring using the Iontronic Sensor

The sensor can be used to record fingertip pulse waves with high stability in dynamic conditions. The high compliance of the materials allows the sensor to be conformally adhered on the curved surface of a fingertip to capture the weak pulse signal. The characteristic waves, including the P-, T-, and D- waves, can be clearly identified (Figure S6, Supporting Information). For traditional pulse monitoring at wrist, the recorded pulses are susceptible to



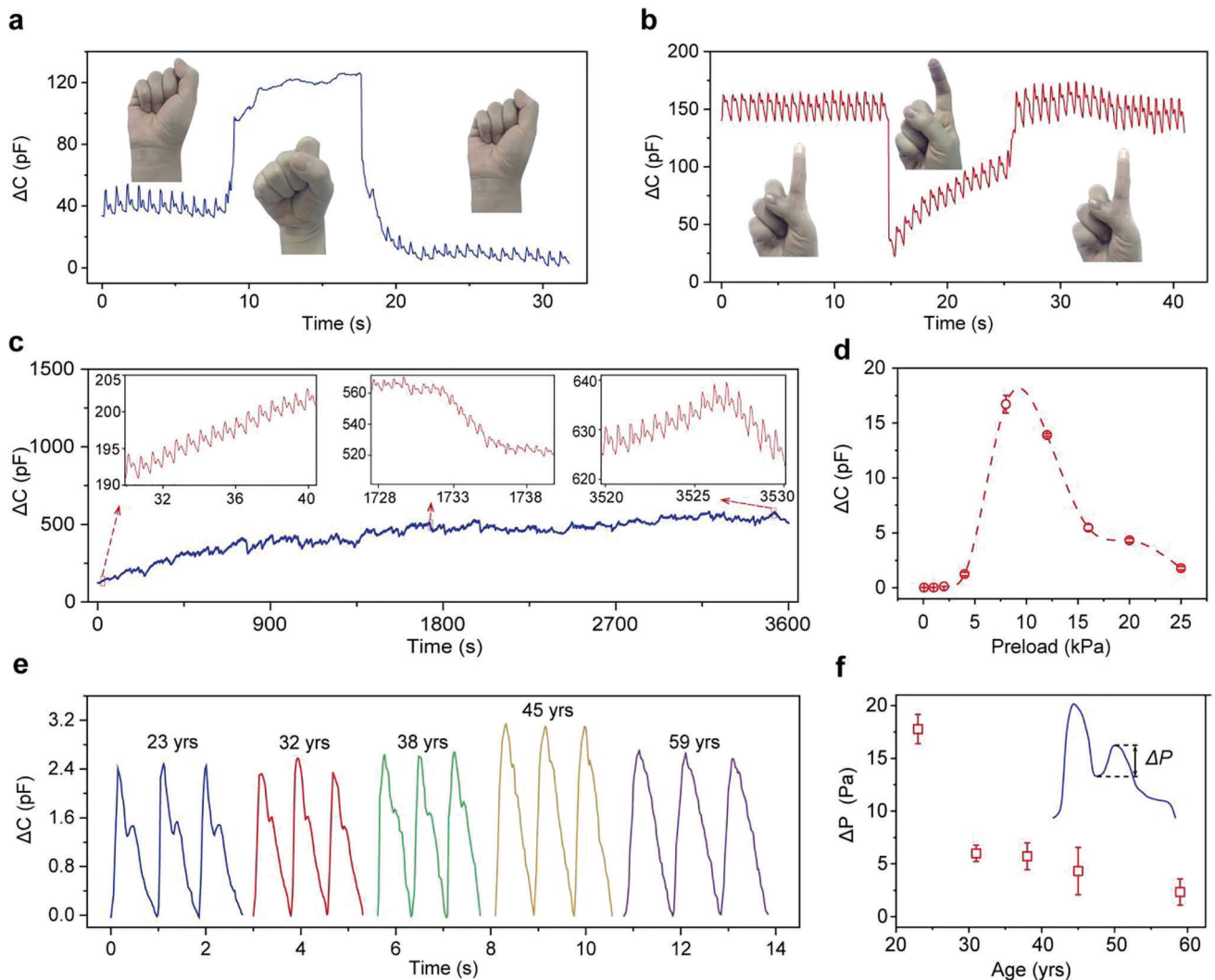


**Figure 3.** Stability and effectiveness of the sensor in pulse monitoring. a) Monitoring of radial artery pulse wave under wrist bending and release. b) Monitoring of fingertip pulse wave under fingertip bending and release. c) Test of fingertip pulse over 1 h. d) The height of the P-wave of a 25-year-old male subject under different preloads. e) Fingertip pulse waveforms of healthy subjects of different ages of 23, 32, 38, 45, and 59. f) The change of  $\Delta P$  (pressure difference between the descending isthmus and the T-wave) with the age of subjects.

motion artifacts because wrist is one of the most flexible joints of human body. The radial artery pulse cannot be clearly recorded when wrist bends forward (Figure 3a), and thus the pulse signal often gets lost during joint motions. In comparison, clear fingertip pulse waves are recorded during finger bending or straightening, although there is often a drift of baseline (Figure 3b). The result indicates that the pulse monitoring at fingertip is barely affected by gestures. The high stability to body motion can last for a long period of time. This is evidenced in Figure 3c, which shows continuous monitoring of pulse wave without any signal loss within 1 h for a 26-year-old male subject.

We investigated the effect of preload on wave amplitude of the fingertip pulse to determine a desired test condition. The preload was controlled precisely using a commercial blood pressure gauge. The wave amplitude (height of the P-wave) increases as the preload increases from 60 to 10 kPa for a 25-year-old

male subject. When the preload exceeds 10 kPa, however, the signal magnitude begins to decrease with increasing preload (Figure 3d), and irregular waves appear as the preload increases to 25 kPa (Figure S7, Supporting Information). We therefore select 10 kPa as the preferred preload for our test.

We recorded the fingertip pulse of several healthy volunteer subjects of different ages to evaluate the accuracy and reliability of the pressure sensor in pulse sensing (Figure 3e). Because the arterial wall usually becomes stiffer with age, the reflected wave occurs earlier and the intensity of the wave decreases. As a result, the T-wave moves upward and becomes less clear with the increase of age. We define the pressure difference between the first descending isthmus and the peak of the T-wave as  $\Delta P$ , which reflects the trend of the change in T-wave. It is found that  $\Delta P$  decreases as age increases, with a minimum value of  $\approx 2.3$  Pa at the age of 60 (Figure 3f). Such a small pressure difference can be well

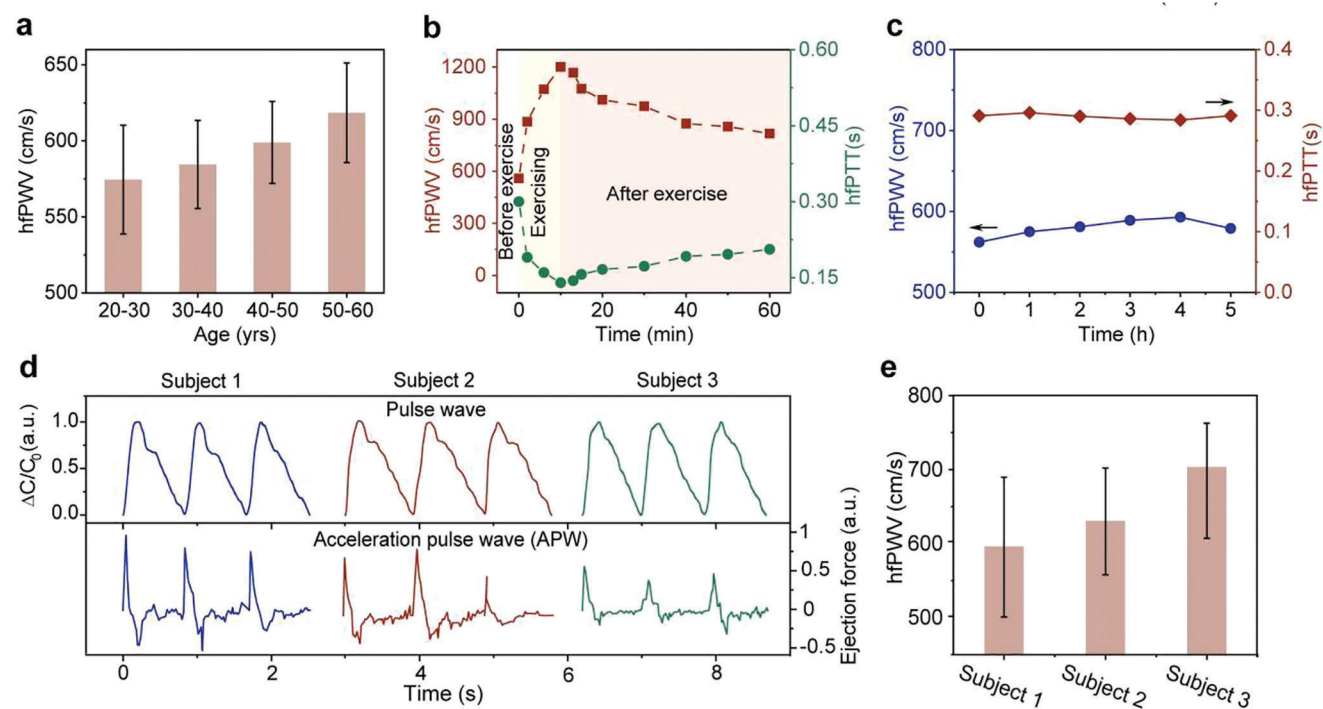


**Figure 4.** Acquisition of hfPWV through the fingertip pulse measurement using the iontronic sensor. a) Change of hfPWV with the age of subjects. b) Changes of hfPWT and hfPTT of a 25-year-old male subject before, in, and after exercise. c) Long term test (5 h) of hfPWV and hfPTT of the 25-year-old subject. d) Fingertip pulse waves and corresponding acceleration pulse waves of a 52-year-old healthy subject, a 53-year-old subject with mild arteriosclerosis, and a 46-year-old subject with serious arteriosclerosis. The last two have been diagnosed in hospital via the traditional method. e) Comparison of hfPWV of the three subjects.

detected because our sensor exhibits a pressure-resolution as low as 0.2 Pa under a preload of 10 kPa, which is below the  $\Delta P$  values of all subjects (Figure 2e).

## 2.4. Acquisition of hfPWV Using Fingertip Pulse Waves

The APW can be obtained through quadratic differentiation of the pulse wave. The time interval between the first two peaks of the hfAPW wave is denoted as hfPTT. The heart-to-fingertip round-trip arterial length ( $S$ ) is related to the subject height, forearm length, and hand length.<sup>[34]</sup> The hfPWV value is determined by dividing  $S$  with hfPTT. We investigated the dependence of hfPWV on the age of the subjects (aged between 20 and 60), who were grouped by age, with each group spanning 10 years. Despite the dramatic differences in cardiovascular conditions of individuals, the average hfPWV value of each group generally increases with age, indicating an increased arterial stiffness (Figure 4a). This trend is attributed to the progression of arterial elasticity with age, which degrades progressively due to the accumulation of metabolic products.

The effect of exercise on pulse waveform was also investigated based on the data of a 25-year-old male subject. Fingertip pulse waves of the subject before, in, and after exercise are shown in Figure S8 (Supporting Information). The hfPPT value decreases from 0.30 (before exercise) to 0.14 s during exercise, and rises slowly to the original value after exercise. Accordingly, the hfPWV value increases sharply from 560 to 1200  $\text{cm s}^{-1}$ , and falls gradu-

ally during rest (Figure 4b). The variation of hfPTT and hfPWV in this process corresponds to the metabolic status of the subjects, which indicates that our sensor can reliably monitor the hfPWV during body motion. Furthermore, the measured hfPWV of the subject in static conditions is generally stable over 5 h (Figure 4c), showing the potential of our sensor in continuous monitoring of arterial stiffness.

The fingertip pulse is potential for the monitoring and assessment of arteriosclerosis. Three male subjects with ages of 52, 53, and 46 were involved in the test, who were clinically diagnosed in hospital as normal, mild arteriosclerosis, and serious arteriosclerosis, respectively. We select subjects with similar ages so that the influence of age can be largely excluded. We measured fingertip pulse waves of the subjects, showing that the T-wave moves upward and its peak height decreases with the aggravation of arteriosclerosis degree (Figure 4d). The hfPTT values of the three subjects were read from their APW waves (Figure 4d). Accordingly, the measured hfPWV value rises from subject 1 to subject 3 (Figure 4e). The results verify that the PWV values measured using our sensor are in accordance with the traditional medical diagnosis of arteriosclerosis.

## 2.5. HfPWV-Based Model for Arteriosclerosis Assessment

According to the principle of Omron colin-automatic arteriosclerosis detector (BP-203RPEIII), the degree of arteriosclerosis is clinically divided into four stages based on the baPWV value

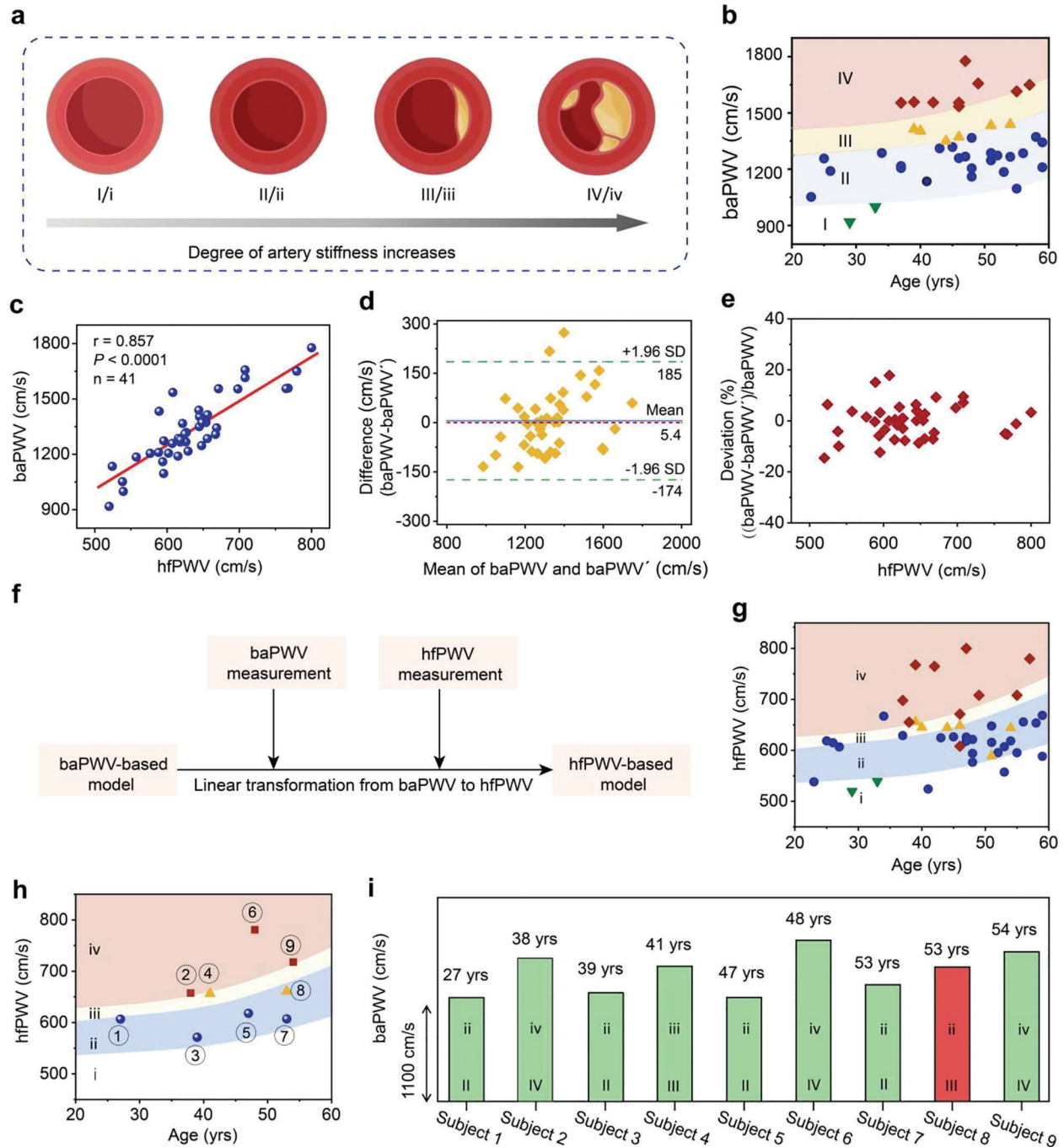


**Figure 5.** Comparison between the models for arteriosclerosis assessment based on hfPWV and baPWV measurements. a) Degrees of arteriosclerosis: soft (I/i), normal (II/ii), mild sclerosis (III/iii) and severe sclerosis (IV/iv). b) baPWV and age values of 41 volunteers, which determine the degree of arterial stiffness. c) Correlation between hfPWV and baPWV. d) Bland-Altman figure of baPWV and hfPWV. e) Deviation of baPWV and hfPWV. f) A simplified diagram for the transformation from the baPWV-based model to the hfPWV-based model. g) Degrees of arteriosclerosis of the 41 subjects in the hfPWV-based model. h) Degree of arteriosclerosis of the other 9 volunteers in the hfPWV-based model. i) Comparison between the baPWV and the hfPWV-based models in determining the degree of arteriosclerosis for the 9 volunteers.

and age: soft (I), normal (II), mild sclerosis (III), and severe sclerosis (IV) (Figure 5a).<sup>[35]</sup> Since the intrinsic arterial stiffness usually increases with age, the boundaries between neighboring stages bend up with increasing age (Figure 5b). We measured the baPWV values of 41 volunteer subjects aged between 20 and 60

and classified their degree of arteriosclerosis by baPWV and age, as shown in Figure 5b. The hfPWV values of the 41 subjects were also measured and proven to be valid to assess the arteriosclerosis level using the single-point method. We used the Pearson correlation coefficient ( $r$ ), which is a common statistical measure



of two variables, to discuss the correlation between hfPWV and baPWV. The value of  $r$  closer to 1 indicates a strong correlation, while the value closer to 0 indicates little correlation. Here, the  $r$  value of hfPWV-baPWV is 0.857 (Figure 5c), which means that the two types of PWV values are linearly correlated and have a strong correlation.

We use a linearly transformed parameter of baPWV (denoted as baPWV') following a fitted function of  $\text{baPWV}' = a \times \text{hfPWV} + b$  ( $a = 2.37$ ,  $b = -183$ ) to validate the correlation between the baPWV-based and the hfPWV-based criteria (Figure 5c). The consistency between baPWV' and baPWV is studied using the Bland-Altman plot (Figure 5d), which is a common mathematical tool to characterize the agreement between two medical parameters.<sup>[36,37]</sup> For each pair of baPWV and baPWV', the mean value and the difference between the two parameters were displayed as the points in an X-Y chart. The average of the difference ( $\bar{D}$ ) for all points is  $5.4 \text{ cm s}^{-1}$ , and the agreement range is between  $-174$  and  $184 \text{ cm s}^{-1}$  ( $\bar{D} \pm 1.96 \text{ SD}$ ). Since 95.1% of the sample points (39/41) falls within the agreement range that exceeds the threshold of reliability estimation (95%), the consistency between the baPWV and baPWV' is determined to be high. Because baPWV' is a linear transformation of hfPWV, it can be concluded that hfPWV is also highly consistent with baPWV. We also studied the deviation between baPWV and hfPWV in Figure 5e. For each sample point, the  $x$  value is hfPWV, and the  $y$  value is the normalized difference between baPWV and baPWV'. Our result indicates that 37 out of 41 (90.2%) sample points fall within the 10% deviation range, and the maximum deviation of all sample points is 17.8%. We therefore conclude that hfPWV, which is measured using a single-point method, can serve as a reliable alternative to the clinical parameter baPWV.

We further establish a model for arteriosclerosis assessment based on the hfPWV values. The boundary curves of the new model were determined using the least squares method:

$$\begin{bmatrix} P_1 \\ P_2 \end{bmatrix}^* = \underset{i=1}{\text{argmin}} \sum^n (P_1 \cdot x_i + P_2 - y_i)^2 = (X^T X)^{-1} X^T Y \quad (2)$$

where  $P_1$  and  $P_2$  represent the slope and the vertical intercept of linear fitting equation between baPWV and hfPWV, respectively,  $x_i$  represents the baPWV value of sample  $i$ ,  $y_i$  represents the corresponding hfPWV value,  $X$  represents the augmented matrix of all  $x_i$ ,  $X^T$  represents transposed matrix of  $X$ ,  $Y$  represents the column vector of all  $y_i$ . Figure 5f shows a simplified diagram that is transformed from the baPWV-based model to the hfPWV-based model, with details of the transformation provided in Scheme S1 (Supporting Information). In short, the data points of baPWV and hfPWV were used to build a fitting algorithm to achieve maximum correspondence of their section, for which the optimal proportion coefficient can be determined. Next, the proportion coefficient was multiplied with the boundary curve coordinates of the baPWV-based model as the boundary curve of the hfPWV-based model. The hfPWV-based model also contains four stages (i, ii, iii, and iv, corresponding to stages I, II, III, and IV in traditional methods) for assessing the degree of arteriosclerosis (Figure 5g), with a shape of each domain being similar to that of the baPWV-based model (Figure 5b).

We verify the validity of the hfPWV-based model by comparing with the baPWV-based model in evaluating the degree of arteriosclerosis. Nine subjects with baPWV values distributed in stage II, III, and IV were selected for comparison (Figure 5h,i). The hfPWV-based model gives a close result: eight out of the nine subjects are consistent in both models, while only subject 8 falls in stage (III) of the baPWV-based model and stage (ii) of the hfPWV-based model (close to the boundary of stage (ii) and stage (iii)). Note that this subject is in a special condition: he is diabetic and suffers from the numbness of lower limbs. Therefore, the hfPWV value, which mainly reflects the arteriosclerosis degree of the upper limbs, is expected to be more reliable than the baPWV-based assessment for this specific case. Overall, our study suggests that the hfPWV-based model is valid and reliable in assessing the degree of arteriosclerosis, and further optimization of the model can be conducted by enlarging the sample capacity and refining the boundaries of different stages.

### 3. Conclusion

In summary, we have developed a high-performance iontronic pressure sensor and a single-point method for the measurement of PWV, a critical indicator of arteriosclerosis. The high performance sensor enables accurate recording of the fingertip pulse waves and the computation of hfPTT and hfPWV. The single-point hfPWV measurement can be applied in both static and dynamic conditions, and shows high stability in continuous PWV monitoring for at least 5 h. We further established a hfPWV-based model and verified that this model agrees well with the state-of-the-art clinical criterion based on baPWV, and is expected to be a reliable technique for arteriosclerosis assessment.

### 4. Experimental Section

**Preparation of Microstructured Ionic Gel:** The resin mold with a pre-defined peanut-groove array was printed using a high-precision 3D printer (NanoArch S130, BMF Precision Tech. Inc.) with a spatial precision of  $2 \mu\text{m}$  and layer thickness of  $5 \mu\text{m}$ . The PDMS precursor with a base to curing agent (Sylgard 184, Dow Corning Co., Ltd) weight ratio of 10:1 was coated onto the resin mold and cured at  $80 \text{ }^\circ\text{C}$  for 1 h. After curing, PDMS with complementary surface patterns was peeled off, serving as the template for casting microstructured ionic gel.

The precursors of ionic gel, PVA-1799 and phosphoric acid (AR,  $\geq 85\%$ ) were purchased from Aladdin Reagent (Shanghai) Co., Ltd. Eight grams of PVA-1799 was added in 72 g of deionized water and stirred at  $95 \text{ }^\circ\text{C}$  for 2 h. Next, the mixture was cooled to  $60 \text{ }^\circ\text{C}$  and mixed with 10.7 g of phosphoric acid. After stirring for 1 h, 0.6 g of the solution was casted on the PDMS template with an area of  $4.9 \text{ cm}^2$  and cured at room temperature for 48 h. The solidified ionic gel was  $\approx 100 \mu\text{m}$  in thickness with a replicated peanut-groove array on the surface, which was then peeled off from the PDMS template and cut into a square with a side length of 3 mm ready for use.

**Assembly of Iontronic Pressure Sensors:** The iontronic pressure sensor was prepared by sandwiching the microstructured ionic gel between two flexible electrodes of Au coated polyethylene terephthalate (PET) films. The flexible electrode was prepared by successively depositing a 20-nm-thick platinum film and a 100-nm-thick gold film on a PET film ( $30 \mu\text{m}$ ) via ion sputtering (MC1000, Hitachi High-Tech Co., Ltd.). Finally, the sandwiched structure was packaged using a 100- $\mu\text{m}$ -thick PDMS film.

**Characterization and Measurements:** The surface morphologies of the resin mold and the microstructured ionic gel were characterized by field-emission scanning electron microscopy (Regulus SU8230, Hitachi High-Tech Co., Ltd.). The applied pressure was measured using a mechanical



tester (Model XLD-20E, Jingkong Mechanical Testing Co., Ltd.). The capacitance of the sensor was recorded using a precision LCR meter (E4980AL, Keysight Tech. Co., Ltd) working at a frequency of 10 kHz. The response and relaxation time were determined by adding and removing a weight on the sensor, and the real-time capacitance was recorded using an LCR meter (TH2840B, Tonghui Inc.). Fingertip pulse monitoring was conducted by fixing the sensor on the finger pulp (for measuring the preload).

**Acquisition of PWV Value and Data Processing:** The baPWV values of the subjects were measured directly using an Omron colin-automatic arteriosclerosis detector (BP-203RPEIII). For the acquisition of hfPPT and hfPWV, the measured fingertip pulse ( $\Delta C-t$ ) was quadratically differentiated, which was called APW curve. The interval between the first two peaks of the APW curve was defined as hfPPT. The hfPWV was computed by dividing the round-trip heart-finger distance ( $S$ ) with hfPPT. For fingertip pulse monitoring and baPWV acquisition, the tests were conducted indoor at an ambient temperature of 25 °C.

For investigating the consistency between hfPWV and baPWV, the baPWV-hfPWV scattering diagram was fitted into a straight line through the least square method, and the correlation coefficient ( $r$ ) was automatically given in the procedure. The transformation from the baPWV-based model to the hfPWV-based model was through a polynomial fitting process, with the detailed flow chart shown in Scheme S1 (Supporting Information).

**Experiments on Human Subjects:** Informed consent was given by each human subject and all experiments were conducted under approval from the Institutional Review Board at the Southern University of Science and Technology under the protocol number 20220178.

**Statistical Analysis:** For the built-up of hfPWV-based model, the sample size is 41. For the validation of hfPWV-based model, the sample size is 9. For each subject, the baPWV value was obtained and the fingertip pulse waveform was recorded. Pearson correlation coefficient ( $r$ ) and Bland-Altman plot were used to investigate the correlation of baPWV and hfPWV values. The software used for data analysis included Matlab 2017b and Origin 9.0.

## Supporting Information

Supporting Information is available from the Wiley Online Library or from the author.

## Acknowledgements

Y.H. and L.Z. contributed equally to this work. The work was funded by the National Natural Science Foundation of China (No. T2225017, No. 52073138, and No. 52103301), Scientific Research Program of Shenzhen Nanshan District (No. NS2021030), Special Foundation of The President of SUSTech Hospital (No. 2021-C6), Natural Science Foundation of Guangdong Province (2023A1515012835).

## Conflict of Interest

The authors declare no conflict of interest.

## Data Availability Statement

The data that support the findings of this study are available from the corresponding author upon reasonable request.

## Keywords

arteriosclerosis, fingertip pulses, flexible pressure sensors, iontronic nanointerfaces, pulse wave velocity

Received: June 9, 2023

Revised: August 9, 2023

Published online: August 31, 2023

- [1] T. Sato, K. Maeda, S. Nagataki, T. Yoshida, B. Grefenstette, B. J. Williams, H. Umeda, M. Ono, J. P. Hughes, *Nature* **2021**, 592, 537.
- [2] J. L. M. Björkegren, A. J. Lusic, *Cell* **2022**, 185, 1630.
- [3] G. Bergström, M. Persson, M. Adiels, E. Björnson, C. Bonander, H. Ahlström, J. Alfredsson, O. Angerås, G. Berglund, A. Blomberg, J. Brandberg, M. Börjesson, K. Cederlund, U. d. Faire, O. Duvernoy, Ö. Eklom, G. Engström, J. E. Engvall, E. Fagman, M. Eriksson, D. Erlinge, B. Fagerberg, A. Flinck, I. Gonçalves, E. Hagström, O. Hjelmgren, L. Lind, E. Lindberg, P. Lindqvist, J. Ljungberg, et al., *Circulation* **2021**, 144, 916.
- [4] S. K. Mohanta, L. Peng, Y. Li, S. Lu, T. Sun, L. Carnevale, M. Perrotta, Z. Ma, B. Förstera, K. Stanic, C. Zhang, X. Zhang, P. Szczepaniak, M. Bianchini, B. R. Saeed, R. Carnevale, D. Hu, R. Nosalski, F. Pallante, M. Beer, D. Santovito, A. Ertürk, T. C. Mettenleiter, B. G. Klupp, R. T. A. Megens, S. Steffens, J. Pelisek, H.-H. Eckstein, R. Kleemann, L. Habenicht, et al., *Nature* **2022**, 605, 152.
- [5] Z. Yi, Z. Liu, W. Li, T. Ruan, X. Chen, J. Liu, B. Yang, W. Zhang, *Adv. Mater.* **2022**, 34, 2110291.
- [6] A. R. van Rosendaal, I. J. van den Hoogen, U. Gianni, X. Ma, S. W. Tantawy, A. M. Bax, Y. Lu, D. Andreini, M. H. Al-Mallah, M. J. Budoff, F. Cademartiri, K. Chinnaiyan, J. H. Choi, E. Conte, H. Marques, P. A. Gonçalves, I. Gottlieb, M. Hadamitzky, J. A. Leipsic, E. Maffei, G. Pontone, S. Shin, Y.-J. Kim, B. K. Lee, E. J. Chun, J. M. Sung, S.-E. Lee, R. Virmani, H. Samady, Y. Sato, et al., *JAMA Cardiol.* **2021**, 6, 1257.
- [7] T. Willum-Hansen, J. A. Staessen, C. Torp-Pedersen, S. Rasmussen, L. Thijs, H. Ibsen, J. Jeppesen, *Circulation* **2006**, 113, 664.
- [8] P. A. Sarafidis, C. Loutradis, A. Karpetas, G. Tzanas, A. Piperidou, G. Koutroumpas, V. Raptis, C. Syrgkanis, V. Liakopoulos, G. Efstratiadis, G. London, C. Zoccali, *Hypertension* **2017**, 70, 148.
- [9] Y. Zhang, P. He, Y. Li, Y. Zhang, J. Li, M. Liang, G. Wang, G. Tang, Y. Song, B. Wang, C. Liu, L. Liu, Y. Cui, X. Wang, Y. Huo, X. Xu, X. Qi, *Cardiovasc. Diabetol.* **2019**, 18, 111.
- [10] T. Ohkuma, T. Ninomiya, H. Tomiyama, K. Kario, S. Hoshida, Y. Kita, T. Inoguchi, Y. Maeda, K. Kohara, Y. Tabara, M. Nakamura, T. Ohkubo, H. Watada, M. Munakata, M. Ohishi, N. Ito, M. Nakamura, T. Shoji, C. Vlachopoulos, A. Nagano, O. Yukiyo, T. Kabutoya, K. Asayama, N. Takashima, T. T. Chowdhury, K. Mitsuki-Shinohara, T. Yamashita, *Hypertension* **2017**, 69, 1045.
- [11] S. Parr, B. Scheuermann, S. Hammond, C. J. Ade, *Stroke* **2023**, 54, ATP99.
- [12] M. Okamoto, M. J. Shipley, I. B. Wilkinson, C. M. McEniery, C. A. Valencia-Hernández, A. Singh-Manoux, M. Kivimaki, E. J. Brunner, *Hypertension* **2019**, 74, 929.
- [13] Y. Fang, Y. Zou, J. Xu, G. Chen, Y. Zhou, W. Deng, X. Zhao, M. Roustaei, T. K. Hsiai, J. Chen, *Adv. Mater.* **2021**, 33, 2104178.
- [14] M. Brainin, K. Sliwa, *Lancet* **2020**, 396, 533.
- [15] D. Ato, *Vasc. Health Risk Manag.* **2018**, 14, 41.
- [16] M. Munakata, *Curr. Hypertens. Rev.* **2014**, 10, 49.
- [17] X. Wang, J. Yang, K. Meng, Q. He, G. Zhang, Z. Zhou, X. Tan, Z. Feng, C. Sun, J. Yang, Z. L. Wang, *Adv. Funct. Mater.* **2021**, 31, 2102378.
- [18] K. Meng, S. Zhao, Y. Zhou, Y. Wu, S. Zhang, Q. He, X. Wang, Z. Zhou, W. Fan, X. Tan, J. Yang, J. Chen, *Matter* **2020**, 2, 896.
- [19] Y. Li, Y. Wei, Y. Yang, L. Zheng, L. Luo, J. Gao, H. Jiang, J. Song, M. Xu, X. Wang, W. Huang, *Research* **2022**, 2022, 0002.
- [20] J. Chen, H. Liu, W. Wang, N. Nabulsi, W. Zhao, J. Y. Kim, M.-K. Kwon, J.-H. Ryou, *Adv. Funct. Mater.* **2019**, 29, 1903162.
- [21] Q. Lin, J. Huang, J. Yang, Y. Huang, Y. Zhang, Y. Wang, J. Zhang, Y. Wang, L. Yuan, M. Cai, X. Hou, W. Zhang, Y. Zhou, S. G. Chen, C. F. Guo, *Adv. Healthcare Mater.* **2020**, 9, 2001023.
- [22] H. Osanai, *US Patent* **1984**, 4432374,
- [23] T. Weber, S. Wassertheurer, M. Rammer, A. Haiden, B. Hametner, B. Eber, *Hypertension* **2012**, 60, 534.

- [24] J. Su, A. D. Hughes, U. Simonsen, L. S. Howard, *Circ.: Cardiovasc. Interventions* **2018**, *11*, e006242.
- [25] Y. Fu, S. Zhao, L. Wang, R. Zhu, *Adv. Healthcare Mater.* **2019**, *8*, 1900633.
- [26] J. E. Schwartz, P. U. Feig, J. L. Izzo Jr., *Hypertension* **2019**, *74*, 111.
- [27] W. W. Nichols, S. J. Denardo, I. B. Wilkinson, C. M. McEniery, J. Cockcroft, M. F. O'Rourke, *J Clin Hypertens* **2008**, *10*, 295.
- [28] K. Meng, X. Xiao, W. Wei, G. Chen, A. Nashalian, S. Shen, X. Xiao, J. Chen, *Adv. Mater.* **2022**, *34*, 2109357.
- [29] S. Koyama, H. Ishizawa, K. Fujimoto, S. Chino, Y. Kobayashi, *Sensors* **2017**, *17*, 48.
- [30] M. Elgendi, I. Norton, M. Brearley, D. Abbott, D. Schuurmans, *Biomed. Eng. Online* **2014**, *13*, 139.
- [31] J. Huang, Z. Chen, J. Yuan, C. Zhang, H. Chen, W. Wu, Z. Chen, Y. Liu, M. Zheng, S. Chen, S. Wu, Y. Chen, *Med. Sci. Monit.* **2019**, *25*, 5241.
- [32] L. Gao, M. Wang, W. Wang, H. Xu, Y. Wang, H. Zhao, K. Cao, D. Xu, L. Li, *Nano-Micro Lett.* **2021**, *13*, 140.
- [33] N. Bai, L. Wang, Q. Wang, J. Deng, Y. Wang, P. Lu, J. Huang, G. Li, Y. Zhang, J. Yang, K. Xie, X. Zhao, C. F. Guo, *Nat. Commun.* **2020**, *11*, 209.
- [34] G. Novo, J. F. Sánchez-Muñoz-Torrero, J. F. Calderón-García, J. M. De-Nicolás-Jiménez, L. García-Ortiz, E. Rodilla-Salas, M. A. Gómez-Marcos, C. Suárez-Fernandez, S. Cordovilla-Guardia, S. Rico-Martín, *PLoS One* **2018**, *13*, e0206434.
- [35] L. Chen, X. Liu, L. Jia, Z. Dong, Q. Wang, Y. Chen, Y. Wang, Y. Zheng, S. Nie, K. Song, D. Zhao, S. Duan, Z. Li, Z. Feng, X. Sun, G. Cai, W. Zhang, X. Chen, *Biomed Res. Int.* **2020**, *2020*, 9795240.
- [36] J. R. Weir-McCall, L. Brown, J. Summersgill, P. Talarczyk, M. Bonnici-Mallia, S. C. Chin, F. Khan, A. D. Struthers, F. Sullivan, H. M. Colhoun, A. C. Shore, K. Aizawa, L. Groop, J. Nilsson, J. R. Cockcroft, C. M. McEniery, I. B. Wilkinson, Y. Ben-Shlomo, J. G. Houston, *Hypertension* **2018**, *71*, 937.
- [37] D. Kracht, R. Shroff, S. Baig, A. Doyon, C. Jacobi, R. Zeller, U. Querfeld, F. Schaefer, E. Wühl, B. M. W. Schmidt, A. Melk, *Am. J. Hypertens.* **2011**, *24*, 1294.